Acoustic Meta-holograms for Encrypted Information Transmission

Xudong Fan, Yifan Zhu, Ning Li, Chunsheng Weng, Badreddine Assouar

Acoustic Meta-holograms for Encrypted Information Transmission

Xudong Fan,[1, 2, *] Yifan Zhu,[3] Ning Li,[1] Chunsheng Weng,[1] and Badreddine Assouar[4, †]

[1] *National Key Laboratory of Transient Physics, Nanjing University of Science and Technology, Nanjing 210094, China*
[2] *Key Laboratory of Modern Acoustics, MOE, Nanjing University, Nanjing 210093, China*
[3] *Jiangsu Key Laboratory for Design and Manufacture of Micro-Nano Biomedical Instruments, School of Mechanical Engineering, Southeast University, Nanjing 211189, China*
[4] *Université de Lorraine, CNRS, Institut Jean Lamour, F-54000 Nancy, France.*

(Dated: September 29, 2023)

We report on the theoretical, numerical and experimental investigation of secure acoustic holography. This secure holography is achieved via an encoded hologram generated by a transducer array decoded by a transmissive acoustic meta-key. An unreadable image is received if directly using the encoded hologram, while the desired image can be obtained only with the aid of a decoding metastructure, i.e., a correctly decoding meta-key. The proposed meta-key consists of a series of unit cells, each of them is composed of a straight channel decorated with several opening panels. By adjusting the opening size of unit cells within the meta-key, its transmitted phase profile can be effectively controlled, hence, the desired decoding meta-key can be successfully constructed. The patterns of a butterfly, sunglasses and the letters of NJUST are chosen as examples to demonstrate the performance of the secure acoustic holography. Vulnerability tests of the meta-key further confirm the safety and reliability of secure acoustic holography. With the advantages of simple design, flexible functionality, and high quality for reconstructed images, our work opens a new avenue for acoustic holography and may find applications in secure acoustic communications based on holograms.

I. INTRODUCTION

Acoustic holograms, with the ability of arbitrary sound field reconstruction, have been broadly studied in the last few years, [1–12] offering new inspirations in a variety of applications such as ultrasonic therapy and particle manipulations. [13–18] Holograms are generally realized by either active transducer arrays [3–5, 9] or passive acoustic metamaterials [6–8, 19–21], where the phase and/or amplitude response on each hologram pixel are engineered to re-construct the desired field at a certain spatial location.

For conventional acoustic meta-holograms, the phase plate containing phase information is used for the field reconstruction [1, 2], and the corresponding image quality is, however, barely satisfactory due to the missing amplitude information of holograms. To overcome this limitation, acoustic meta-holograms could be realized based on both phase and amplitude information [7, 22] so that high-quality images can be re-constructed with no need for optimizations. This extraordinary success has broadened the potential applications for acoustic holograms.

At the same time, remarkable progress has been made to achieve holographic images with high efficiency and quality using electromagnetic waves in terahertz, infrared, and visible regimes. [23–35] The electromagnetic meta-holograms can be effectively tuned by controlling either metasurfaces composed of active materials or incident light sources. For the former, different types of external stimuli are generally applied to active metasurfaces to tune meta-holograms such as electrical,[36] thermal, [37] chemical, [38] and mechanical [39] methods. However, for the latter, a single metasurface could be recycled to produce tunable holographic images by controlling different properties of incident light sources, for example, the polarization states, [40] orbital angular momentum, [41] wavelength, [42] incident light angle [43] and coding incident beams.[44] A more comprehensive review for tunable or dynamic electromagnetic meta-holography refer to [45].

The rapid development and great success in electromagnetic meta-holograms provide a promising potential for information storage and encryption,[46–51] and also inspires the acoustic encryption based on holograms. Holographic acoustic encryption, once achieved, will dramatically extend the application scenarios, such as encrypted acoustic information communications, acoustic field reconstruction, [1, 7] acoustic cloaking [52] or illusion,[53] architectural acoustics,[54] and particle manipulations [4, 5, 55].

In this work, we report a framework for secure acoustic holograms with the advantages of secure projection, simple design, flexible functionality, and high quality for reconstructed images. For secure acoustic holography, the desired image is obtained only with the aid of an acoustic meta-key containing the correct decoding information, otherwise producing unreadable images. Here, an acoustic speaker array consisting of 16×16 air-coupled ultrasonic transducers is used to generate the encoded hologram containing both amplitude and enciphered phase information of the transmitted image. The independent modulation of amplitude and phase for

* fanxudong@njust.edu.cn
† badreddine.assouar@univ-lorraine.fr

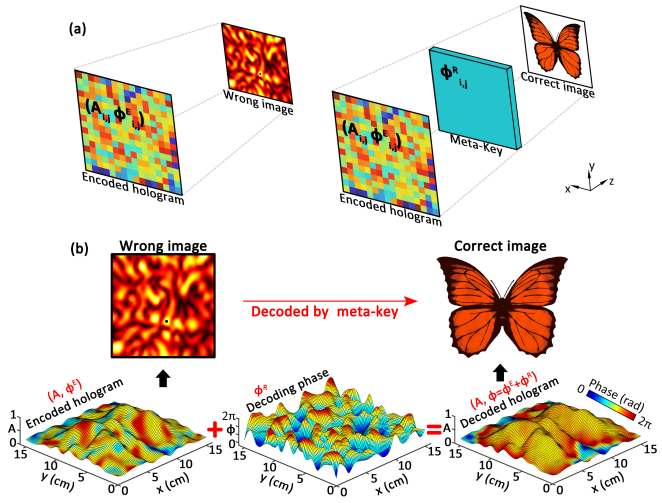

FIG. 1. Illustration of secure acoustic holography. (a) Encoded hologram contains the secure amplitude and enciphered phase information of the transmitted acoustic field, and an unreadable acoustic field will be generated directly using the encoded hologram (left panel). The acoustic meta-key contains the decoding phase, and the desired field can be recovered with the aid of the meta-key. (b) Encoded hologram, decoding phase provided by the meta-key and decoded hologram for the acoustic field of a butterfly.

the speaker array provides extreme flexibility for image reconstruction. A new class of unit cells that could effectively modulate transmitted phase shifts of acoustic waves is designed and used to construct the acoustic meta-key. The reusable meta-key is used to decipher the secure information and recover several changeable predesigned images with high fidelity. The patterns of a butterfly, sunglasses and the letters of NJUST are chosen as examples to demonstrate the concept of secure acoustic holography proposed here. Our work provides a conceptual advance for secure acoustic communications based on holograms.

II. PRINCIPLE OF SECURE HOLOGRAPHY

Figures 1(a) and (b) show the illustration of secure acoustic holography. A desired holographic pattern is arbitrarily chosen first, for example, a butterfly here, and then the pattern is captured by the acoustic pressure field, denoted by, $P(x, y, z)$. In order to reconstruct this image via an acoustic hologram, the time-reversal method [7] is used to calculate the complex pressure profile on the hologram plane, $p(x, y) = A(x, y) \exp[\phi(x, y)]$, which is discretized into two individual $N \times N$ matrices, i.e., $A_{i,j}$ and $\phi_{i,j}$ with $i, j = 1, 2, ..., N$. These two matrices contain all correct amplitude and phase information of the transmitted field.

For the secure acoustic holography, a $N \times N$ random phase matrix is first generated, where every phase element $\phi^{\mathrm{R}}_{i,j}$ within the matrix is randomly generated and obeys the uniform distribution (i.e., $\phi^{\mathrm{R}}_{i,j} \sim [0, 2\pi]$). This random phase matrix is the stochastic code containing the coding information and must be kept confidential. The hologram containing all correct information of the transmitted field will be then enciphered into an encoded hologram based on the random phase matrix. The coding rules are that the amplitude information on the encoded hologram $A^{\mathrm{E}}_{i,j}$ remains unchanged, i.e.,

$$A^{\mathrm{E}}_{i,j} = A_{i,j}, \tag{1}$$

however, the encoded phase information $\phi^{\mathrm{E}}_{i,j}$ is modulated as

$$\phi^{\mathrm{E}}_{i,j} = \phi_{i,j} - \phi^{\mathrm{R}}_{i,j}. \tag{2}$$

As a result, only an unreadable acoustic image (characterized by the acoustic field) can be obtained if directly using the encoded hologram [left panel in Fig. 1(a)].

In order to obtain the desired image, the encoded hologram has to be deciphered first. Here, we design an acoustic decoding meta-key such that it provides exactly the same additional phase as the pre-created random matrix, i.e., $\phi^{\mathrm{R}}_{i,j}$. Consequently, the acoustic waves generated by the encoded hologram will propagate through the acoustic meta-key, and the additional phase information provided by the meta-key will be added to the original encoded information. Finally, the desired image can be obtained based on the decoded hologram [right panel in Fig. 1(a)].

Details for the computation of acoustic holograms are shown below. A holographic pattern is first characterized by the acoustic pressure field, $P(x, y, z)$, where only the amplitude field is taken into consideration and the phase distribution is kept uniform. The field is then discretized into a collection of pixels, $P_m(x_m, y_m, z_m) = A_m(x_m, y_m, z_m)$, where m denotes the pixel number and the uniform phase is chosen to be 0. Hence, the complex acoustic pressure information on the hologram $p_{i,j} = A_{i,j}e^{\phi_{i,j}}$ can be obtained based on the time-reversal method,[7]

$$p_{i,j} = A_{i,j}e^{\phi_{i,j}} = \sum_{m=1}^{M} \frac{A_m}{r_m} \exp(ikr_m), \tag{3}$$

where $k = 2\pi f/c$ is the wavenumber, $c = 343\ \mathrm{m \cdot s^{-1}}$ is the sound speed of the background medium, air. M is the total number of image pixels, and r_m is the spatial distance between the image pixel and hologram pixel, i.e., $r_m^2 = (x_{i,j} - x_m)^2 + (y_{i,j} - y_m)^2 + (z_{i,j} - z_m)^2$.

Inversely, the acoustic field on the image plane can be also calculated analytically based on the information contained in the hologram, i.e.,

$$P_m = \sum_{i,j=1}^{N} \frac{A_{i,j}}{r_{i,j}} \exp[-i(kr_{i,j} - \phi_{i,j})], \tag{4}$$

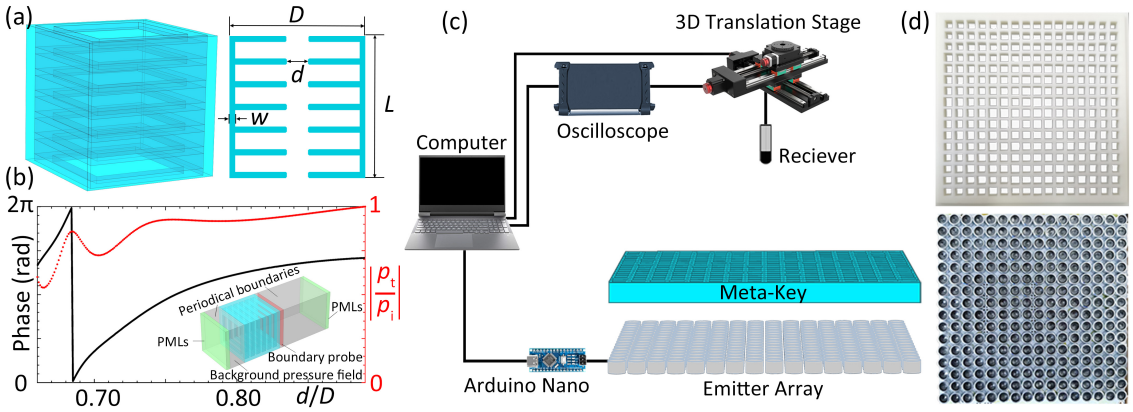

FIG. 2. Illustration of the acoustic meta-key and experiment setup for the measurements of acoustic fields. (a) three-dimensional illustration and the corresponding two-dimensional cross-section of an element of the meta-key. (b) Phase shift and the transmission rate of the sound field when varying the geometry parameter of the element. Inset: simulation setup for the unit of acoustic meta-key. (c) The emitter array consisting of 16×16 elements is connected to a computer through an Arduino Nano board. An ultrasonic receiver is mounted on a translation stage, which is directly controlled by the computer through a Matlab script. Received signals are captured by the oscilloscope and then transmitted to the computer. (d) Photos of a meta-key sample and the emitter array.

where $N \times N$ is the total number of hologram pixels, and the distance $r_{i,j}$ between the spatial point (x, y, z) and the hologram pixel $(x_{i,j}, y_{i,j}, z_{i,j})$ is calculated by $r_{i,j}^2 = (x - x_{i,j})^2 + (y - y_{i,j})^2 + (z - z_{i,j})^2$.

III. DESIGN OF ACOUSTIC META-KEY

The acoustic meta-key is composed of a series of three-dimensional unit cells made of solid materials, as shown in Fig. 2(a). Each unit cell consists of a straight channel decorated with a series of panels. The size of each unit cell is chosen as 10 mm × 10 mm × 10 mm. The wall thickness of the structure is $w = 0.5$ mm, and the opening size of panels d is adjusted to control the transmitted phase shift of acoustic waves (similar structures refer to [56–58]).

Numerical results of the phase shift and the corresponding transmission rate $|p_t/p_i|$ of the transmitted sound field through the unit cell are shown in Fig. 2(b), where p_i and p_t are the incident and the transmitted acoustic pressures. From the results, the transmitted phase shift (black solid line) can cover the span of 2π when varying the geometry parameter d/D while keeping the transmission rate (red dots) at a high level.

Here, numerical simulations are conducted on a server (equipped with the AMD Ryzen Threadripper 3970X 32-Core Processor with 128GB of memory) using the "Acoustic-Thermoviscous Acoustic Interaction, Frequency Domain" module in COMSOL Multiphysics, which is commercial software based on the finite element method [see Inset in Fig. 2(b)]. Perfectly matched layers (PMLs) are used for the outer boundaries of the computation domain to prevent undesired reflections. Free tetrahedral mesh with a maximum size of $\lambda/5$ is used within the main computation domain, and a mapped mesh of 8 layers is used for the perfectly matched layers. Particularly, a finer mesh is configured near boundary layers to obtain acoustic fields precisely. The walls of the acoustic structure are set as sound-hard boundaries. The background pressure field is used with a working frequency of 40 kHz, which is the same as the operating frequency of the speaker array. The mass density and the sound speed of background medium air are set as $\rho_0 = 1.21$ kg·m^{-3}, and $c_0 = 343$ m·s^{-1}, respectively. The transmitted phase shift of acoustic waves is obtained by the average sound pressure on the transmitted plane (Boundary probe in the simulation setup).

The experiments are carried out in a three-dimensional space with the illustration shown in Fig. 2(c). A speaker array consisting of 16×16 air-coupled ultrasonic transducers of 1 cm-diameter (Murata MA40S4S, driven by a 12 V peak-to-peak square wave signal and producing a sinusoidal output at 40 kHz) is used as the source, and another air-coupled ultrasonic transducer (Murata MA40S4S) is placed at a distance of 15 cm behind the sample of acoustic meta-keys as a receiver. The receiver is connected to a translation stage, which directly communicates with a laptop through a Matlab script. The scanning area at the image plane is 15.4×15.4 cm^2 with a scanning resolution of 2 mm. The data from the receiver is collected through the oscilloscope (PicoScope 54444D) to the laptop for further operations. The enlarged photos for the speaker array and the meta-key are shown in Fig. 2(d). The meta-key containing the decoding information is designed based on the random phase matrix [59]. Here, all the samples are made of photosensitive resin and are manufactured via the three-dimensional printing technique (Lite600HD, 0.1 mm in precision). Each meta-key consists of 16×16

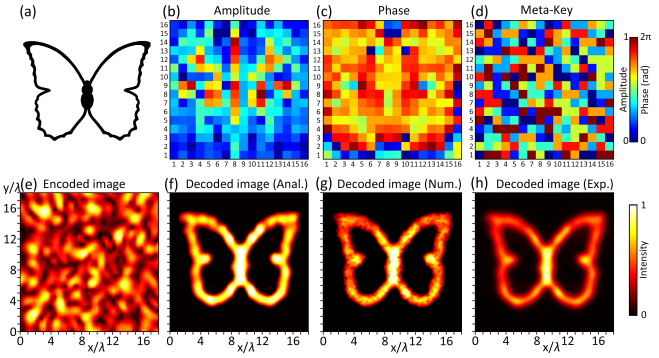

FIG. 3. Results for the field of a butterfly. (a) Desired field of a butterfly. (b) Encoded amplitude and (c) phase information for the desired field. (d) Additional phase provided by the meta-key. (e) Unreadable field generated directly by the encoded hologram. (f-h) Analytical, numerical, and experimental results for the field generated by the decoded hologram.

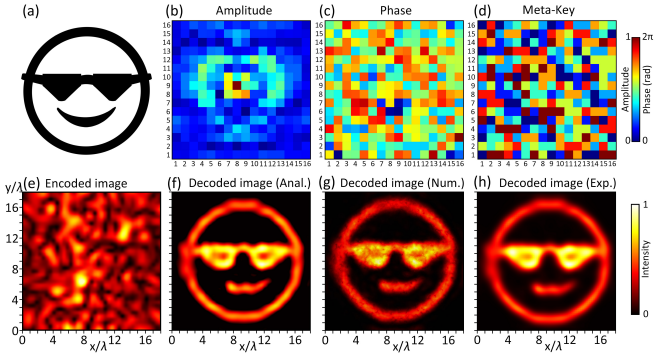

FIG. 4. Results for the field of sunglasses. (a) Desired field of sunglasses. (b) Encoded amplitude and (c) phase information for the desired field. (d) Additional phase provided by the meta-key. (e) Unreadable field generated directly by the encoded hologram. (f-h) Analytical, numerical, and experimental results for the field generated by the decoded hologram.

unit cells with the sample size of 16 cm × 16 cm × 1 cm.

IV. SECURE ACOUSTIC HOLOGRAPHY

Holographic Image of a Butterfly. To demonstrate the secure acoustic hologram proposed here, a holographic image of a butterfly as shown in Fig. 3(a) is first chosen as an example. The amplitude and phase information on the encoded hologram is calculated based on Eqs. (1)-(3) as shown in Figs. 3(b) and (c), and the random phase matrix is generated with the results shown in Fig. 3(d). Here, N is chosen as 16, and the distance between the image plane and the hologram plane is 15 cm, i.e., $z_m = 15$ cm, and $z_{i,j} = 0$ cm. The source employed in our experiments is a speaker array consisting of 16 × 16 air-coupled ultrasonic transducers, where the initial amplitude and phase of each speaker can be adjusted individually so that both the amplitude and phase information on the encoded hologram can be directly achieved by the speaker array. Another air-coupled ultrasonic transducer is placed at a spatial distance of 15 cm away from the hologram to receive transmitted signals. The acoustic field directly generated by the encoded hologram is shown in Fig. 3(e), where an unreadable image is obtained as expected.

In order to access the desired image, the information contained within the encoded hologram must be deciphered first. Hence, here an acoustic meta-key possessing the confidential stochastic code, i.e., the previous random phase profile [Fig. 3(d)], is designed and placed in front of the speaker array. The acoustic waves generated by the encoded hologram will pass through the meta-key, and the enciphered information is then decoded and deciphered.

Figures 3(f-h) present acoustic intensity distribution on the image plane for the analytical results based on Eq. (4), the numerical simulation based on the finite element method, and the experimental measurements, respectively. From the results, the pre-designed pattern of a butterfly is clearly observed after being deciphered by the meta-key, proving the excellent performance of the secure acoustic holography proposed here, and also validating the ability of the meta-key to generate high-quality acoustic holograms.

Holographic Image of sunglasses. In order to demonstrate the flexibility of the proposed secure acoustic hologram, another holographic image of sunglasses, is presented here [Fig. 4(a)]. Similarly, the amplitude and phase information on the encoded hologram is calculated based on Eqs. (1)-(3) with the results shown in Figs. 4(b) and (c). The random phase matrix containing the coding information is shown in Fig. 4(d), which is the same as that in Fig. 3(d). Here, as long as the random phase matrix (i.e., the stochastic code) is still secure and confidential, it can be kept unchanged. Otherwise, a new random matrix must be re-generated to keep the information secret.

The acoustic field directly generated by the encoded hologram is shown in Fig. 4(e), where an unreadable image is again obtained as expected. Then, the previous meta-key possessing the same stochastic code is placed in front of the speaker array to decode the enciphered information contained in the encoded hologram.

Figures 4(f-h) exhibit acoustic intensity distribution on the image plane for the analytical results [Eq. (4)], the numerical simulation, and the experimental measurements, respectively. From the results, the pre-designed pattern of sunglasses is clearly observable, proving the high fidelity and confidentiality of the secure acoustic holography proposed here.

Holographic Image of the Letters NJUST. In order to further demonstrate the flexibility of the secure acoustic hologram proposed, another holographic image

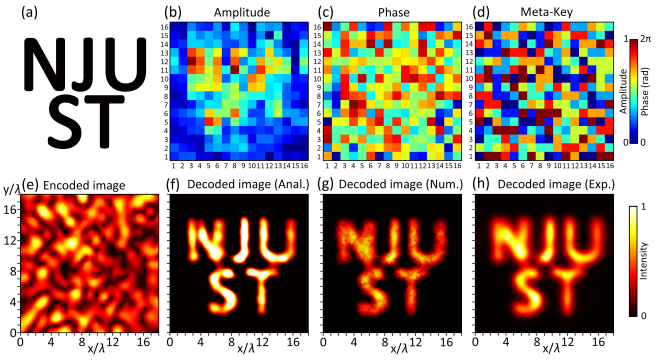

FIG. 5. Results for the field of the letters, NJUST. (a) Desired field of NJUST. (b) Encoded amplitude and (c) phase information for the desired field. (d) Additional phase provided by the meta-key. (e) Unreadable field generated directly by the encoded hologram. (f-h) Analytical, numerical, and experimental results for the field generated by the decoded hologram.

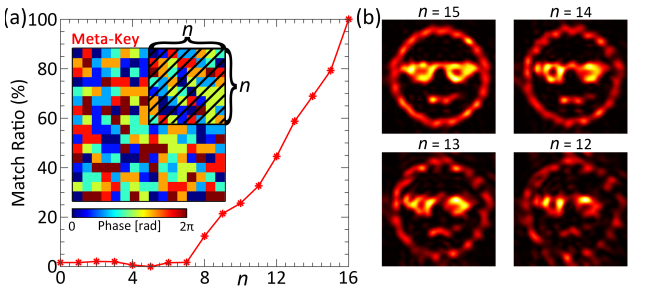

FIG. 6. The vulnerability test of the meta-key. (a) Match ratio between the holographic images using the partial meta-key and the entire meta-key. Inset: partial meta-key (marked by the shadow) containing $n \times n$ effective phases. (b) Intensity fields using partial meta-keys with different n.

of the letters, NJUST, is presented here [Fig. 5(a)], where multiple letters are transmitted on a single holographic image. Similarly, the amplitude and phase information on the encoded hologram is calculated based on Eqs. (1)-(3) with the results shown in Figs. 5(b) and (c). The random phase matrix containing the coding information is shown in Fig. 5(d).

The acoustic field directly generated by the encoded hologram is shown in Fig. 5(e), where an unreadable image is again obtained as expected. Then, the previous meta-key possessing the same stochastic code is placed in front of the speaker array to decode the enciphered information contained in the encoded hologram. Figures 5(f-h) show acoustic intensity distribution on the image plane for the analytical results [Eq. (4)], the numerical simulation, and the experimental measurements, respectively. From the results, the pre-designed pattern of letters NJUST is well recovered and clearly observed.

V. VULNERABILITY TEST OF THE META-KEY

We have experimentally shown that different meta-holograms can be realized using the same meta-key (see Figs. 3-5), and the transmitted information can be protected when the meta-key is mistakenly accessed by others. In order to examine the security and reliability of the meta-key, the vulnerability of the proposed concept of secure acoustic holography has been tested when a whole part of the meta-key is accessed by others (Fig. 6). The match ratio between the meta-holographic images using the partial meta-key and the entire meta-key is shown in Fig. 6(a), where the match ratio decreases with the area of the partial meta-key characterized by n [the deciphered part of the meta-key is marked by the shadow in the inset in Fig. 6(a)]. The reconstructed image becomes fuzzy even when a major part of the meta-key is used [$n = 15$; see Fig. 6(b)], and the image of sunglasses is hard to identify when n is reduced to 12. Here, the match ratio is obtained by $(1 - \text{N-RMSE}) \times 100\%$, where N-RMSE represents the normalized root mean squared error of the image reconstructed using a partial meta-key, and the match ratio reaches 100% if using the whole meta-key. Therefore, the frame of secure acoustic holography proposed here exhibits pretty good performance for security even though almost the simplest encryption method is used for the decoding meta-key.

To further test the security of the system, another situation, when the specific information on some of its random locations is deciphered, is considered (Fig. 7). The deciphered parts of the meta-key are illustrated by shadows in the inset in Fig. 7(a), where the area ratio between the deciphered part and the whole meta-key is characterized by the decryption percentage. The match ratio between the meta-holographic images using the partial meta-key and the entire meta-key is shown in Fig. 7(a), where the match ratio increases with the decryption percentage. The reconstructed image is still fuzzy even when 85% of the meta-key is deciphered [Fig. 7(b)], and the image is barely recognized when the decryption percentage reaches 90%, which again confirms the security and reliability of the secure acoustic holography proposed here; see Video 1 for the dynamic evolution of the reconstructed holographic images when the information of the meta-key is deciphered [59].

We have also examined the effect of the image location on the quality of the reconstructed hologram. Figure 8 shows the reconstructed images at different spatial locations in z direction. The meta-holographic image becomes blurry when the deviation of the image plane from the preset location is larger than 2λ. This spatial location of the image plane provides us with another degree of freedom for information encryption in addition to the transmitted encrypted amplitude and

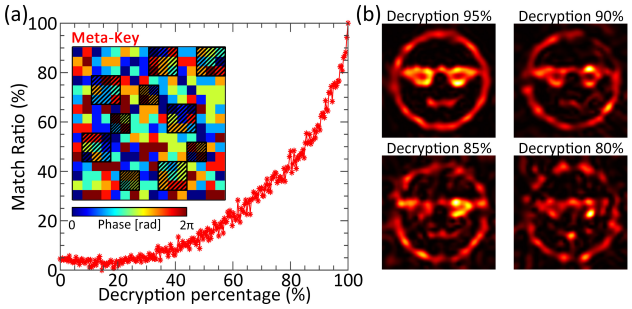

FIG. 7. The vulnerability test of the meta-key when the information at random locations is deciphered. (a) Match ratio between the holographic images using the partial meta-key and the entire meta-key. Inset: the partially-deciphered meta-key is illustrated by shadows. (b) Intensity fields using partially-deciphered meta-keys.

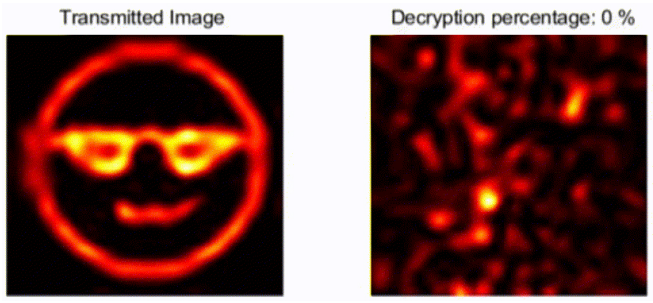

Video 1. Dynamic evolution of the reconstructed holographic images when the information of the meta-key is deciphered.

phase information and the secure meta-key [59].

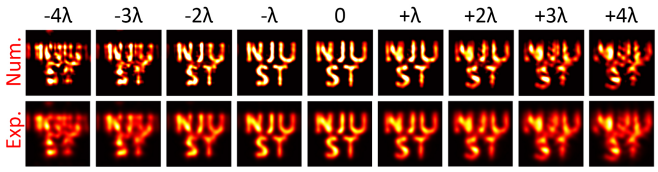

FIG. 8. Experimental and analytical results for NJUST at different positions in z direction. The corresponding values above images indicate the distance between the image plane and the predesigned location.

VI. CONCLUSION

In summary, we have proposed and investigated a framework for secure acoustic holography. The latter is achieved via an encoded hologram decoded by a transmissive acoustic meta-key. An acoustic speaker array consisting of 16×16 air-coupled ultrasonic transducers has been used to generate the encoded hologram containing both amplitude and enciphered phase information. An unreadable image is received if directly using the encoded hologram, and the desired image can be obtained only with the aid of the correctly decoding meta-key. A new class of unit cells that could effectively modulate transmitted phase shifts of acoustic waves was designed and used to build the acoustic meta-key, which can decode the enciphered information and recover the predesigned images with high fidelity. As a proof of concept, we analytically, numerically, and experimentally demonstrated secure acoustic holography for the patterns of a butterfly, sunglasses, and the letters of NJUST. The results exhibit pretty good performance for security even when a majority part of the meta-key is deciphered. Our work provides a framework for secure acoustic communications with the advantages of simple design, flexible functionality, and high quality for reconstructed images. The results could be beneficial for a variety of acoustic applications involving secure communications and underwater communications where optical and electromagnetic counterparts may not be the first option.

For the secure acoustic holography proposed here, a fixed meta-key can be recycled as long as the random phase information contained in the meta-key is still secure and confidential. Since a simple encryption strategy of the random phase distortion is used here, there is still a chance for the proposed method to be potentially deciphered using some optimization methods, for example, phase retrieval methods under a certain amount of iterations [60]. However, more complex encryption strategies of the meta-key could be easily extended based on the framework proposed here. In addition, meta-keys capable of both amplitude and phase modulations can be considered to further improve the security of the system.

ACKNOWLEDGMENTS

This work is supported by the National Natural Science Foundation of China (Grant No. 12204241), the Natural Science Foundation of Jiangsu Province (Grant No. BK20220924), and the Fundamental Research Funds for the Central Universities (Grants No. 30923011019 and No. 020414380195).

[1] Kai Melde, Andrew G Mark, Tian Qiu, and Peer Fischer, "Holograms for acoustics," Nature **537**, 518–522 (2016).
[2] Yangbo Xie, Chen Shen, Wenqi Wang, Junfei Li, Dingjie Suo, Bogdan-Ioan Popa, Yun Jing, and Steven A Cummer, "Acoustic holographic rendering with two-dimensional metamaterial-based passive phased

array," Scientific reports **6**, 35437 (2016).
[3] Asier Marzo, Sue Ann Seah, Bruce W Drinkwater, Deepak Ranjan Sahoo, Benjamin Long, and Sriram Subramanian, "Holographic acoustic elements for manipulation of levitated objects," Nature communications **6**, 1–7 (2015).
[4] Asier Marzo and Bruce W Drinkwater, "Holographic acoustic tweezers," Proceedings of the National Academy of Sciences **116**, 84–89 (2019).
[5] Ryuji Hirayama, Diego Martinez Plasencia, Nobuyuki Masuda, and Sriram Subramanian, "A volumetric display for visual, tactile and audio presentation using acoustic trapping," Nature **575**, 320–323 (2019).
[6] Ye Tian, Qi Wei, Ying Cheng, and Xiaojun Liu, "Acoustic holography based on composite metasurface with decoupled modulation of phase and amplitude," Applied Physics Letters **110**, 191901 (2017).
[7] Yifan Zhu, Jie Hu, Xudong Fan, Jing Yang, Bin Liang, Xuefeng Zhu, and Jianchun Cheng, "Fine manipulation of sound via lossy metamaterials with independent and arbitrary reflection amplitude and phase," Nature communications **9**, 1–9 (2018).
[8] Shi-Wang Fan, Yifan Zhu, Liyun Cao, Yan-Feng Wang, A-Li Chen, Aurélien Merkel, Yue-Sheng Wang, and Badreddine Assouar, "Broadband tunable lossy metasurface with independent amplitude and phase modulations for acoustic holography," Smart Materials and Structures **29**, 105038 (2020).
[9] Ryuji Hirayama, Diego Martinez Plasencia, Nobuyuki Masuda, and Sriram Subramanian, "A volumetric display for visual, tactile and audio presentation using acoustic trapping," Nature **575**, 320–323 (2019).
[10] Mingxin Xu, William S Harley, Zhichao Ma, Peter VS Lee, and David J Collins, "Sound-speed modifying acoustic metasurfaces for acoustic holography," Advanced Materials , 2208002.
[11] Shubhi Bansal, Christabel Choi, James Hardwick, Biswajoy Bagchi, Manish K Tiwari, and Sriram Subramanian, "Transmissive labyrinthine acoustic metamaterial-based holography for extraordinary energy harvesting," Advanced Engineering Materials , 2201117 (2022).
[12] Jin Zhang, Ye Tian, Ying Cheng, and Xiaojun Liu, "Acoustic holography using composite metasurfaces," Applied Physics Letters **116**, 030501 (2020).
[13] Jinwook Kim, Sandeep Kasoji, Phillip G Durham, and Paul A Dayton, "Acoustic holograms for directing arbitrary cavitation patterns," Applied Physics Letters **118** (2021).
[14] Sergio Jiménez-Gambín, Noé Jiménez, Antonios N Pouliopoulos, José M Benlloch, Elisa E Konofagou, and Francisco Camarena, "Acoustic holograms for bilateral blood-brain barrier opening in a mouse model," IEEE Transactions on Biomedical Engineering **69**, 1359–1368 (2021).
[15] Sergio Jiménez-Gambín, Noé Jiménez, José María Benlloch, and Francisco Camarena, "Holograms to focus arbitrary ultrasonic fields through the skull," Physical Review Applied **12**, 014016 (2019).
[16] Zhichao Ma, Andrew W Holle, Kai Melde, Tian Qiu, Korbinian Poeppel, Vincent Mauricio Kadiri, and Peer Fischer, "Acoustic holographic cell patterning in a biocompatible hydrogel," Advanced Materials **32**, 1904181 (2020).
[17] Zhichao Ma, Hyungmok Joh, Donglei Emma Fan, and Peer Fischer, "Dynamic ultrasound projector controlled by light," Advanced Science **9**, 2104401 (2022).
[18] Zhichao Ma, Kai Melde, Athanasios G Athanassiadis, Michael Schau, Harald Richter, Tian Qiu, and Peer Fischer, "Spatial ultrasound modulation by digitally controlling microbubble arrays," Nature communications **11**, 4537 (2020).
[19] Yangbo Xie, Chen Shen, Wenqi Wang, Junfei Li, Dingjie Suo, Bogdan-Ioan Popa, Yun Jing, and Steven A Cummer, "Acoustic holographic rendering with two-dimensional metamaterial-based passive phased array," Scientific reports **6**, 1–6 (2016).
[20] Michael D Brown, "Phase and amplitude modulation with acoustic holograms," Applied Physics Letters **115**, 053701 (2019).
[21] Chuanxin Zhang, Xue Jiang, Shuai Han, Jiajie He, Yan Zheng, Boyi Li, and Dean Ta, "Converged wireless infrastructure with acoustic holographic array," Applied Physics Reviews **9**, 041413 (2022).
[22] Yifan Zhu and Badreddine Assouar, "Systematic design of multiplexed-acoustic-metasurface hologram with simultaneous amplitude and phase modulations," Physical Review Materials **3**, 045201 (2019).
[23] Haider Butt, Yunuen Montelongo, Tim Butler, Ranjith Rajesekharan, Qing Dai, Sai G Shiva-Reddy, Timothy D Wilkinson, and Gehan AJ Amaratunga, "Carbon nanotube based high resolution holograms," Advanced materials **24**, OP331–OP336 (2012).
[24] Stephane Larouche, Yu-Ju Tsai, Talmage Tyler, Nan M. Jokerst, and David R. Smith, "Infrared metamaterial phase holograms," NATURE MATERIALS **11**, 450–454 (2012).
[25] Benny Walther, Christian Helgert, Carsten Rockstuhl, Frank Setzpfandt, Falk Eilenberger, Ernst-Bernhard Kley, Falk Lederer, Andreas Tuennermann, and Thomas Pertsch, "Spatial and spectral light shaping with metamaterials," ADVANCED MATERIALS **24**, 6300–6304 (2012).
[26] Xingjie Ni, Alexander V Kildishev, and Vladimir M Shalaev, "Metasurface holograms for visible light," Nature communications **4**, 2807 (2013).
[27] Lingling Huang, Xianzhong Chen, Holger Mühlenbernd, Hao Zhang, Shumei Chen, Benfeng Bai, Qiaofeng Tan, Guofan Jin, Kok-Wai Cheah, Cheng-Wei Qiu, et al., "Three-dimensional optical holography using a plasmonic metasurface," Nature communications **4**, 2808 (2013).
[28] Guoxing Zheng, Holger Muehlenbernd, Mitchell Kenney, Guixin Li, Thomas Zentgraf, and Shuang Zhang, "Metasurface holograms reaching 80% efficiency," NATURE NANOTECHNOLOGY **10**, 308–312 (2015).
[29] Dandan Wen, Fuyong Yue, Guixin Li, Guoxing Zheng, Kinlong Chan, Shumei Chen, Ming Chen, King Fai Li, Polis Wing Han Wong, Kok Wai Cheah, Edwin Yue Bun Pun, Shuang Zhang, and Xianzhong Chen, "Helicity multiplexed broadband metasurface holograms," NATURE COMMUNICATIONS **6** (2015), 10.1038/ncomms9241.
[30] Lingling Huang, Holger Muhlenbernd, Xiaowei Li, Xu Song, Benfeng Bai, Yongtian Wang, and Thomas Zentgraf, "Broadband hybrid holographic multiplexing with geometric metasurfaces," ADVANCED MATERIALS **27**, 6444+ (2015).
[31] Lei Wang, Sergey Kruk, Hanzhi Tang, Tao Li, Ivan

Kravchenko, Dragomir N Neshev, and Yuri S Kivshar, "Grayscale transparent metasurface holograms," Optica **3**, 1504–1505 (2016).

[32] Wenyu Zhao, Bingyi Liu, Huan Jiang, Jie Song, Yanbo Pei, and Yongyuan Jiang, "Full-color hologram using spatial multiplexing of dielectric metasurface," OPTICS LETTERS **41**, 147–150 (2016).

[33] Bo Wang, Fengliang Dong, Qi-Tong Li, Dong Yang, Chenawei Sun, Jianjun Chen, Zhiwei Song, Lihua Xu, Weiguo Chu, Yun-Feng Xiao, Qihuang Gong, and Yan Li, "Visible-frequency dielectric metasurfaces for multiwavelength achromatic and highly dispersive holograms," NANO LETTERS **16**, 5235–5240 (2016).

[34] Qiu Wang, Xueqian Zhang, Yuehong Xu, Jianqiang Gu, Yanfeng Li, Zhen Tian, Ranjan Singh, Shuang Zhang, Jiaguang Han, and Weili Zhang, "Broadband metasurface holograms: toward complete phase and amplitude engineering," Scientific reports **6**, 32867 (2016).

[35] Adam C Overvig, Sajan Shrestha, Stephanie C Malek, Ming Lu, Aaron Stein, Changxi Zheng, and Nanfang Yu, "Dielectric metasurfaces for complete and independent control of the optical amplitude and phase," Light: Science & Applications **8**, 92 (2019).

[36] Chengjun Zou, Andrei Komar, Stefan Fasold, Justus Bohn, Alexander A. Muravsky, Anatoli A. Murauski, Thomas Pertsch, Dragomir N. Neshev, and Isabelle Staude, "Electrically tunable transparent displays for visible light based on dielectric metasurfaces," ACS Photonics **6**, 1533–1540 (2019), https://doi.org/10.1021/acsphotonics.9b00301.

[37] Xingbo Liu, Qiu Wang, Xueqian Zhang, Hua Li, Quan Xu, Yuehong Xu, Xieyu Chen, Shaoxian Li, Meng Liu, Zhen Tian, Caihong Zhang, Chongwen Zou, Jiaguang Han, and Weili Zhang, "Thermally dependent dynamic meta-holography using a vanadium dioxide integrated metasurface," ADVANCED OPTICAL MATERIALS **7** (2019), 10.1002/adom.201900175.

[38] Jianxiong Li, Simon Kamin, Guoxing Zheng, Frank Neubrech, Shuang Zhang, and Na Liu, "Addressable metasurfaces for dynamic holography and optical information encryption," SCIENCE ADVANCES **4** (2018), 10.1126/sciadv.aar6768.

[39] Stephanie C. Malek, Ho-Seok Ee, and Ritesh Agarwal, "Strain multiplexed metasurface holograms on a stretchable substrate," NANO LETTERS **17**, 3641–3645 (2017).

[40] Peixia Zheng, Qi Dai, Zile Li, Zhiyuan Ye, Jun Xiong, Hong-Chao Liu, Guoxing Zheng, and Shuang Zhang, "Metasurface-based key for computational imaging encryption," SCIENCE ADVANCES **7** (2021), 10.1126/sciadv.abg0363.

[41] Lei Jin, Yao-Wei Huang, Zhongwei Jin, Robert C. Devlin, Zhaogang Dong, Shengtao Mei, Menghua Jiang, Wei Ting Chen, Zhun Wei, Hong Liu, Jinghua Teng, Aaron Danner, Xiangping Li, Shumin Xiao, Shuang Zhang, Changyuan Yu, Joel K. W. Yang, Federico Capasso, and Cheng-Wei Qiu, "Dielectric multi-momentum meta-transformer in the visible," NATURE COMMUNICATIONS **10** (2019), 10.1038/s41467-019-12637-0.

[42] Inki Kim, Heonyeong Jeong, Joohoon Kim, Younghwan Yang, Dasol Lee, Trevon Badloe, Gyeongtae Kim, and Junsuk Rho, "Dual-band operating metaholograms with heterogeneous meta-atoms in the visible and near-infrared," ADVANCED OPTICAL MATERIALS **9** (2021), 10.1002/adom.202100609.

[43] Seyedeh Mahsa Kamali, Ehsan Arbabi, Amir Arbabi, Yu Horie, MohammadSadegh Faraji-Dana, and Andrei Faraon, "Angle-multiplexed metasurfaces: Encoding independent wavefronts in a single metasurface under different illumination angles," PHYSICAL REVIEW X **7** (2017), 10.1103/PhysRevX.7.041056.

[44] Hui Gao, Yuxi Wang, Xuhao Fan, Binzhang Jiao, Tingan Li, Chenglin Shang, Cheng Zeng, Leimin Deng, Wei Xiong, Jinsong Xia, and Minghui Hong, "Dynamic 3d meta-holography in visible range with large frame number and high frame rate," SCIENCE ADVANCES **6** (2020), 10.1126/sciadv.aba8595.

[45] Jaekyung Kim, Junhwa Seong, Younghwan Yang, Seong-Won Moon, Trevon Badloe, and Junsuk Rho, "Tunable metasurfaces towards versatile metalenses and metaholograms: a review," ADVANCED PHOTONICS **4** (2022), 10.1117/1.AP.4.2.024001.

[46] Jaehyuck Jang, Heonyeong Jeong, Guangwei Hu, Cheng-Wei Qiu, Ki Tae Nam, and Junsuk Rho, "Kerker-conditioned dynamic cryptographic nanoprints," Advanced Optical Materials **7**, 1801070 (2019).

[47] Inki Kim, Jaehyuck Jang, Gyeongtae Kim, Jihae Lee, Trevon Badloe, Jungho Mun, and Junsuk Rho, "Pixelated bifunctional metasurface-driven dynamic vectorial holographic color prints for photonic security platform," Nature Communications **12**, 3614 (2021).

[48] Peixia Zheng, Qi Dai, Zile Li, Zhiyuan Ye, Jun Xiong, Hong-Chao Liu, Guoxing Zheng, and Shuang Zhang, "Metasurface-based key for computational imaging encryption," Science Advances **7**, eabg0363 (2021).

[49] Kevin TP Lim, Hailong Liu, Yejing Liu, and Joel KW Yang, "Holographic colour prints for enhanced optical security by combined phase and amplitude control," Nature communications **10**, 25 (2019).

[50] Yanjun Bao, Ying Yu, Haofei Xu, Chao Guo, Juntao Li, Shang Sun, Zhang-Kai Zhou, Cheng-Wei Qiu, and Xue-Hua Wang, "Full-colour nanoprint-hologram synchronous metasurface with arbitrary hue-saturation-brightness control," LIGHT-SCIENCE & APPLICATIONS **8** (2019), 10.1038/s41377-019-0206-2.

[51] Jianxiong Li, Simon Kamin, Guoxing Zheng, Frank Neubrech, Shuang Zhang, and Na Liu, "Addressable metasurfaces for dynamic holography and optical information encryption," SCIENCE ADVANCES **4** (2018), 10.1126/sciadv.aar6768.

[52] Bogdan-Ioan Popa, Lucian Zigoneanu, and Steven A Cummer, "Experimental acoustic ground cloak in air," Physical review letters **106**, 253901 (2011).

[53] Xu-Dong Fan, Bin Liang, Jing Yang, and Jian-Chun Cheng, "Illusion for airborne sound source by a closed layer with subwavelength thickness," Scientific Reports **9**, 1750 (2019).

[54] Yifan Zhu, Xudong Fan, Bin Liang, Jianchun Cheng, and Yun Jing, "Ultrathin acoustic metasurface-based schroeder diffuser," Physical Review X **7**, 021034 (2017).

[55] Xudong Fan, Yifan Zhu, Zihao Su, Ning Li, Xiaolong Huang, Yang Kang, Can Li, Chunsheng Weng, Hui Zhang, Weiwei Kan, et al., "Transverse particle trapping using finite bessel beams based on acoustic

metamaterials," Physical Review Applied **19**, 034032 (2023).
[56] Xudong Fan, Yifan Zhu, Zihao Su, Ning Li, Xiaolong Huang, Yang Kang, Can Li, Chunsheng Weng, Hui Zhang, Bin Liang, et al., "Ultrabroadband and reconfigurable transmissive acoustic metascreen," Advanced Functional Materials , 2300752 (2023).
[57] Yong Li, Xue Jiang, Bin Liang, Jian-chun Cheng, and Likun Zhang, "Metascreen-based acoustic passive phased array," Physical Review Applied **4**, 024003 (2015).
[58] Liping Ye, Chunyin Qiu, Jiuyang Lu, Kun Tang, Han Jia, Manzhu Ke, Shasha Peng, and Zhengyou Liu, "Making sound vortices by metasurfaces," AIP Advances **6** (2016).
[59] See Supplemental Material at [URL will be inserted by publisher] for the detailed parameters of the meta-key and the vulnerability tests of the meta-key under attack.
[60] Byungjae Hwang, Taeseong Woo, Cheolwoo Ahn, and Jung-Hoon Park, "Imaging through random media using coherent averaging," Laser & Photonics Reviews **17**, 2200673 (2023).